MAJOR MERGERS WITH SMALL GALAXIES: THE DISCOVERY OF A MAGELLANIC-TYPE GALAXY AT $z = 0.12$[*]

Andreas Koch[1,5], Matthias J. Frank[1], Anna Pasquali[2], R. Michael Rich[3,5], and Andreas Rabitz[4]

[1] Zentrum für Astronomie der Universität Heidelberg, Landessternwarte, Königstuhl 12, D-69117 Heidelberg, Germany; akoch@lsw.uni-heidelberg.de
[2] Zentrum für Astronomie der Universität Heidelberg, Astronomisches Rechen-Institut, Mönchhofstrasse 12, D-69117 Heidelberg, Germany
[3] University of California Los Angeles, Department of Physics & Astronomy, Los Angeles, CA, USA
[4] Leibniz-Institut für Astrophysik Potsdam, An der Sternwarte 16, D-14482 Potsdam, Germany

ABSTRACT

We report on the serendipitous discovery of a star-forming galaxy at redshift $z = 0.116$ with morphological features that indicate an ongoing merger. This object exhibits two clearly separated components with significantly different colors, plus a possible tidal stream. Follow-up spectroscopy of the bluer component revealed a low star-forming activity of $0.09\,M_\odot\,\mathrm{yr}^{-1}$ and a high metallicity of $12 + \log(\mathrm{O/H}) = 8.6$. Based on comparison with mass–star formation-rate and mass–metallicity relations, and on fitting of spectral energy distributions, we obtain a stellar mass of $3 \times 10^9\,M_\odot$, which renders this object comparable to the Large Magellanic Cloud. Thus our finding provides a further piece of evidence of a major merger already acting on small, dwarf-galaxy-like scales.

Key words: galaxies: abundances – galaxies: dwarf – galaxies: interactions – galaxies: irregular – galaxies: star formation – galaxies: structure

1. INTRODUCTION

Minor and major mergers are an important source for the hierarchical build-up of large-scale structures such as galaxies. These processes have been prominently traced over a large portion of the universe, from our own Milky Way (MW; ingesting the Sagittarius dwarf galaxy; Ibata et al. 1994) to the immediate vicinity of M 31 (in the form of the Giant Stellar Stream; Ibata et al. 2001; McConnachie et al. 2009), and also in the local universe (Martínez-Delgado et al. 2010; Rich et al. 2012). In all those cases, all participants in the mergers are still resolvable into stars, allowing for detailed studies of the underlying stellar populations. Similarly, dramatic galaxy interactions are observed at larger distances (e.g., Forbes et al. 2003; Conn et al. 2011) and on the scales of galaxy clusters (Koch et al. 2012). Above redshifts of $z \gtrsim 1$, the major merger rate appears to diminish (e.g., Williams et al. 2011).

It remains an intriguing question, down to which scales mergers will play an important role. For instance, there are indications that Fornax, the second-most-massive dwarf spheroidal satellite to the MW, has experienced several major accretion events of gas-rich systems (Hendricks et al. 2014). Moreover, the Large and Small Magellanic Clouds (LMC and SMC, respectively) are likely to have had repeated close interactions, triggering star formation (Harris & Zaritsky 2009) and shaping the warped bar and irregular structure of the LMC

and the associated, gaseous Magellanic Stream (Besla et al. 2012). Based on their orbital characteristics, it has been suggested that both irregular dwarfs had entered the MW system as a binary pair (Kallivayalil et al. 2013).

However, galaxy pairs like the LMC-SMC-MW system are not overly common in the local universe, nor are they predicted in simulations of hierarchical accretion: the occurrence of satellites with a mass of the LMC or above to MW-sized galaxies lies at a mere 12% (Liu et al. 2011; Tollerud et al. 2011; Robotham et al. 2012), consistent with the Millennium simulations of Boylan-Kolchin et al. (2011). Furthermore, the LMC is unusual in that it has a remarkably blue color compared to its peers, both in galaxy groups and in isolation, possibly owing to the merger-induced star formation (Tollerud et al. 2011; Besla et al. 2012).

Given the importance of baryon removal from galaxies during such interactions and the ensuing morphological transformations in the form of extended, gaseous bridges and tails, Magellanic-type irregular galaxies are good candidates to be targeted in H I surveys. Likewise, many spectroscopic and imaging surveys exist to investigate the star-forming nature of merging and regular galaxies, and to study the evolution of galaxies from the local universe out to large redshifts, connecting stellar masses with the star formation and gas and dust properties as well as with morphology (e.g., Driver et al. 2009; Overzier et al. 2009; Eales et al. 2010; van der Wel et al. 2011).

Here we report on the serendipitous discovery of a low-mass galaxy that shows clear evidence of an ongoing merger event. This paper is organized as follows. In Section 2 we introduce the discovery imaging data and spectroscopic follow-up. Section 3 describes the photometric characterization, while Section 4 is dedicated to the spectroscopic measurements in terms of star formation rate (SFR), metallicity, and stellar mass estimates. These are then discussed in Section 5, where we draw a parallel to the properties of the LMC, before summarizing our findings in Section 6.

Table 1
Photometric Characteristics of J021904 from SDSS

Filter	Magnitude[a]
u	-20.84 ± 0.24
g	-19.63 ± 0.04
r	-18.89 ± 0.04
i	-18.37 ± 0.03
z	-17.99 ± 0.08
M_g	-20.53 ± 0.15[b]

Notes.
[a] Total model magnitude from SDSS, obtained from an exponential profile fit, within 3 $r_e \sim 12''$.
[b] Adopting the luminosity distance of 559 Mpc.

2. DATA

2.1. Wisconsin–Indiana–Yale–NOAO (WIYN) Images

We detected the galaxy, J021904.69+200615.4 (shortened to J021904 in the following), first in imaging of the Segue 2 ultrafaint dwarf spheroidal (cf. Belokurov et al. 2009) we obtained with the 3.5 m Wisconsin–Indiana–Yale–NOAO (WIYN[6]) telescope on Kitt Peak on 2010 October 07. Here, we used the MIMO mosaic camera, which provides a large field of view of $9'.6 \times 9'.6$ spread over two detectors, each with a pixel scale of $0''.14$. Our exposure times were 6×300 s in each V and I and 9×300 s in B, with individual exposures dithered across the gaps. The seeing was $1''$ on average.

Our standard data reduction was carried out in IRAF. The field around Segue 2 is covered by the Sloan Digital Sky Survey (SDSS; Alam et al. 2015). Thus, to photometrically calibrate our data, we used SExtractor (Bertin & Arnouts 1996) to obtain aperture photometry and aperture corrections for stars in the stacked B, V, and I images. The instrumental magnitudes of $\sim$240 stars were then matched against the SDSS DR12 photometric catalog that had been transformed to the Johnson–Cousins BVI system using the photometric transformations of Jordi et al. (2006). For reference, Table 1 lists the photometry of the extended galaxy J021904 listed in SDSS. In SDSS, the total magnitudes were obtained from the best-fit exponential profile, while a de Vauculeurs profile yielded low likelihoods. These magnitudes in SDSS are based on integrating this profile out to three scale radii, or $\sim12''$ (see also Section 3.1), which fully captures the flux from both merger components.

In Figure 1 we show the intensity maps from our BVI imaging. J021904 was discovered as an amorphous, extended system showing clear signs of a double-core structure, most prominently on the B-image, and a possible tidal tail emerging on the southeast side of the galaxy, indicative of an ongoing merger event (Figure 1). Comparison with the MMT images of Belokurov et al. (2009) and the SDSS images indicates that the features in question, while less pronounced on those shallower images, are real and not artifacts of our imaging or reduction procedures.

It is noteworthy that the eastern component is much redder than the western one, which we highlight in Figure 2 in terms of the $B-I$ color map of J021904. The entire object has a visual, radial extent of $\sim8''$ (Figures 1, 2; see also Section 3),
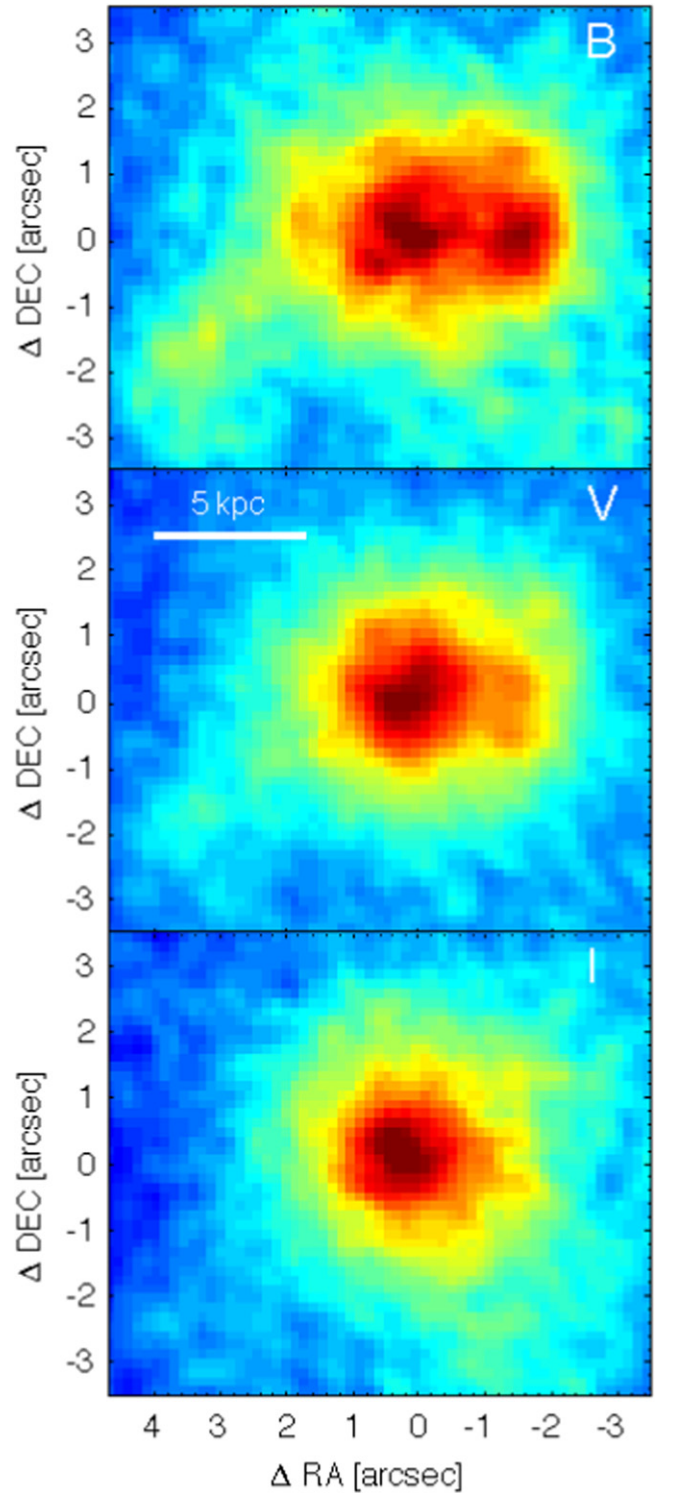
---

[6] The WIYN Observatory is a joint facility of the University of Wisconsin–Madison, Indiana University, Yale University, and the National Optical Astronomy Observatory.

Figure 1. Top to bottom: B, V, and I-band intensity maps of the galaxy J021904. Two components are clearly visible in the B-band image. The images have been smoothed with a Gaussian kernel of $1''$. A scale bar of 5 kpc is indicated. North is up, and east is left.

whereas we note that SDSS lists a Petrosian radius for J021904 of $7''.1 \pm 3''.8$.

2.2. MODS Spectroscopy

We obtained follow-up spectroscopy with the first Multi-object Double Spectrograph (MODS1; Pogge et al. 2010) at the
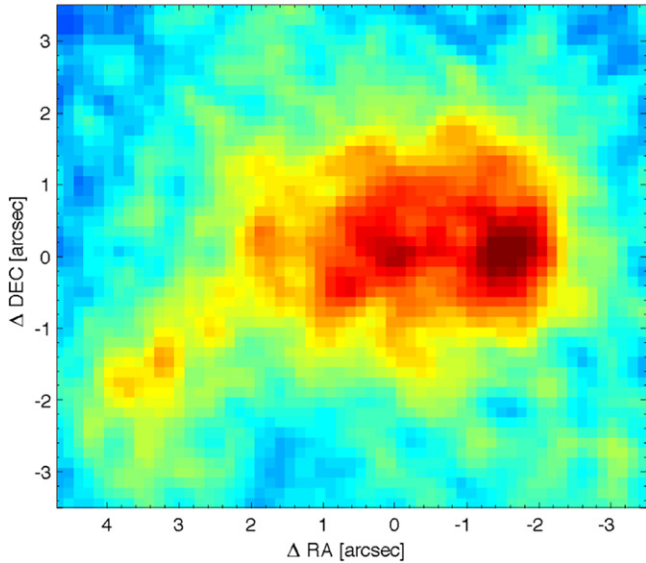
Figure 2. $B-I$ color map of the same region as in Figure 1, highlighting the color difference between the two components. This map have been smoothed with a Gaussian kernel of $1''$.

Figure 3. Combined BVI intensity map of the surroundings of J021904. A red rectangle indicates the placement of the MODS slit. Three additional objects with derived redshift z and stellar heliocentric radial velocity, v_{HC}, from our spectroscopy are also labeled.

Large Binocular Telescope (LBT) on 2012 November 18. While four slit masks for multi-object spectroscopy had been designed so as to representatively cover many subcomponents of the target galaxy, only one could be observed due to unfortunate weather conditions. Here, the slit was placed on the western, bluer component of the galaxy (Figure 3).

In practice, we used a single $1'' \times 10''$ slit and exposed for 5×1800 s to facilitate cosmic ray removal. The chosen setup resulted in a full spectral coverage of 3000–9000 Å at a resolution of $R = 1300$ as measured from the sky lines. We used the MODSCCDRED package[7] for basic data reduction, i.e., bias-removal, and applied pixel-flats. Since small shifts in spatial and wavelength directions between individual exposures were present, we opted to reduce the individual science frames independently. For this, cosmic rays were identified using a python variant[8] of the L.A. Cosmic algorithm (van Dokkum 2001). We then used the MODSIDL pipeline[9] to trace slits, derive the wavelength calibration from day-time arc lamp exposures, perform sky-subtraction on the two-dimensional images (using the method of Kelson 2003), and to extract one-dimensional spectra. Absolute flux calibration was reached via exposure of the spectrophotometric standard star GD 71. For each slit, the spectra extracted from the individual exposures were then combined using an inverse-variance weighted mean. As a result, the signal-to-noise ratio in the continuum near Hα is ~10 per pixel.

The placement of additional slits in the immediate surroundings of the galaxy of interest also allowed us to characterize several fore- and background objects (labeled in Figure 3). Two of these were identified as background galaxies at $z = 0.527$ (with prominent Ca II HK absorption) and $z = 0.288$ (an emission line galaxy). Likewise, the object West
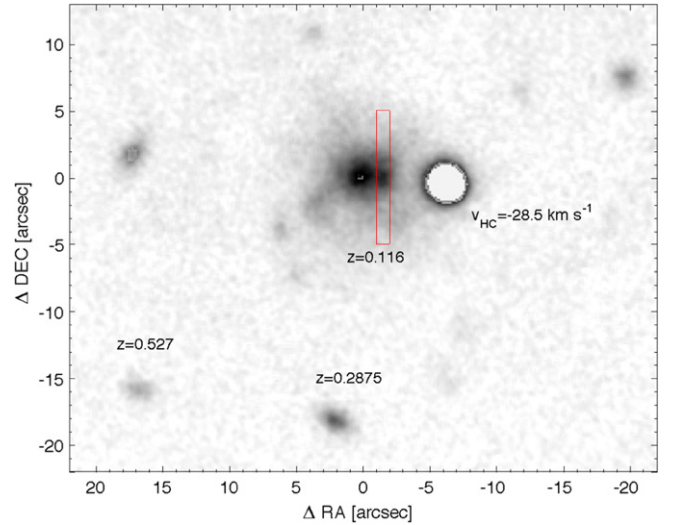
---

7   MODSCCDRED by R. W. Pogge, available at http://www.astronomy.ohio-state.edu/MODS/Software/modsCCDRed/
8   COSMICS.PY by M. Tewes, available at http://obswww.unige.ch/~tewes/cosmics_dot_py/
9   MODSIDL by K. V. Croxall & R. W. Pogge, available at http://www.astronomy.ohio-state.edu/MODS/Software/modsIDL/

Table 2
Derived Photometric Parameters of J021904

Parameter	Value			Notes
	B	V	I	
μ_E [mag/$\square''$]	24.34 ± 0.08	23.44 ± 0.12	22.94 ± 0.34	1
μ_W [mag/$\square''$]	24.52 ± 0.08	23.73 ± 0.13	23.47 ± 0.36	2
r_e [$''$]	4.1 ± 1.7	3.7 ± 0.9	3.5 ± 1.2	3
C	3.6	3.6	3.5	4
A	0.15	0.17	0.13	4
S	0.13	0.28	0.16	4

Note. (1) Central surface brightness of the eastern (redder) component. (2) Central surface brightness of the western (bluer) component. (3) Effective radius of the exponential profile fitted to the entire galaxy. (4) Concentration, Asymmetry, and Smoothness, as defined by Conselice et al. (2000).

of J021904 (at $g = 19.4$ mag) has a heliocentric radial velocity of $v_{HC} = -28$ km s^{-1}. This compares to the systemic velocity of the Segue 2 dwarf galaxy of -40 km s^{-1} and its internal velocity dispersion of 3.4 km s^{-1} (Belokurov et al. 2009), which renders this object a clear foreground star.

3. PHOTOMETRIC MEASUREMENTS

As our surface-brightness measurements on the center of either component of the galaxy indicate, both sides have comparable brightnesses in the B-band, while the western part is considerably fainter, by ~0.6 mag/$\square''$, in the I-band (see Table 2).

Using Herschel observations of local dwarf galaxies, Clark et al. (2015) found a large fraction of objects with remarkably blue colors (albeit in FUV $- K_S$). Similar to J021904, those galaxies show an irregular morphology. Furthermore, Clark et al. (2015) pointed out that those, overall bluer galaxies are dominated by dust and that they are the most actively star-forming galaxies of their survey. This could indicate that the western, bluer component (albeit in the optical bands considered here) of the merger we observed was contributed by a galaxy with a larger dust fraction than the other partner.
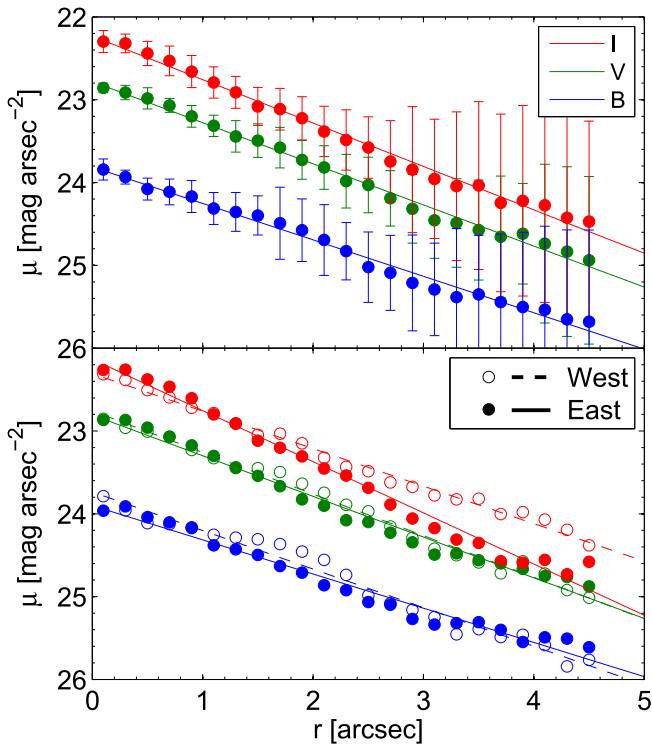
Figure 4. Azimuthally averaged surface-brightness profiles of J021904 from our *B*, *V*, and *I* images (top panel). The bottom panel shows the profiles when restricting to the western ($\xi \leqslant 0$) and eastern ($\xi > 0$) halves. Best-fit exponential profiles are indicated for each subset.

The separation between the centers of the two blobs is $1''6$, corresponding to 3.5 kpc at the distance of J021904 (Section 4.1). Several knots are detected, at the 1σ-level above the background, toward the southeast on the $B-I$ map at projected distances of 7.5, 9, and 10.3 kpc, but at the low spatial resolution of the images it remains inconclusive if they are localized star-forming regions, tidal streams, or accreting dwarf galaxies. Stellar and/or gaseous streams in the Local Group reach lengths of >140 kpc (e.g., Ibata et al. 2001), which, depending on the inclination angle to the observer, could be seen as similar features to what we observe in our target galaxy. Likewise, dwarf satellites to Magellanic galaxies at projected distances of ~ 10 kpc are common (e.g., Rich et al. 2012), so the observed knots could in fact be the relics of an accreted dwarf galaxy.

3.1. Radial Profiles

In Figure 4 we show the azimuthally averaged surface-brightness profiles of J021904 in each of the targeted filters. To this end, we have carefully masked out the nearby star (cf. Figure 3). The best-fit exponential profiles are also shown, yielding consistent effective radii within the error bars (Table 2). For consistency with SDSS (Section 2.1), we use the parameterization $I(R) = \exp(-1.68\,r/r_{\rm e})$ in the following, where $\mu = -2.5 \log I$ and $r_{\rm e}$ denote the effective scale radius containing half of the light. While the difference is not statistically significant, we nonetheless point out that the radius obtained in the *B*-band is in fact the largest, owing to the contribution from the secondary merger component in the brightness distribution. The radii thus obtained correspond to 7.6–9.1 kpc at the distance of the galaxy (Section 4.1). We also

attempted Sérsic fits, but the resulting indices of 0.98–1.05 are fully consistent with an exponential light distribution in this galaxy, also in line with the preponderance of disk-like main-sequence galaxies at higher redshifts (Wuyts et al. 2011). Furthermore, avoiding the seeing disk by restricting the fits to $r > 1''$ had only a negligible influence on the results in that the best-fit radii increased by less than 5% when using the outer regions only. This is much smaller than the uncertainties on the best-fit parameters (Table 2).

In order to look for systematic differences between either component of the double-peaked galaxy, we divided our images into an eastern and a western component and show the resulting profiles in the bottom panel of Figure 4. Also here we tested the effects of seeing by using only data beyond $1''$ and found an 8% (2%) increase (decrease) in the scale radii in the eastern (western) halves. Here it is noteworthy that the profiles in the *V*-band are essentially indistinguishable. While the existence of the second brightness peak is clearly visible between $1''$ and $2''$ in the blue, western profile, the formal best-fit radius is larger on the eastern side by $0''3$, owing to the presence of the purported tidal extension. In contrast the faintness of these features in the reddest filters renders the scale radius of J021904 considerably smaller, by $1''1$. Thus the accreting system or tidal tail could indicate a merger with a bluer object or ongoing star formation in localized regions, possibly triggered by the merger.

3.2. CAS Parameters

In order to further parameterize the morphology and extent of the disturbances of J021904, we determined the "CAS" parameters (Conselice 2003), viz., the galaxy's concentration (C), asymmetry (A), and Clumpiness (S), which are also known to correlate with galaxy type and/or color. Here, we followed the formalism of Conselice et al. (2000) in measuring these parameters from our images.

(1) *Concentration:* C is defined as the logarithmic ratio of those radii that contain 80% and 20% of the cumulative flux contained within a certain Petrosian radius, more specifically, within $1.5 \times r(\eta = 0.2)$, where η denotes the ratio of the local surface brightness to the average surface brightness within radius r (e.g., Djorgovski & Spinrad 1981; Kent 1985; Bershady et al. 2000). Thus,

$$C = 5 \times \log(r_{80\%}/r_{20\%}). \qquad (1)$$

For our galaxy we found $C = (3.6, 3.6, 3.5)$ in *B*, *V*, and *I*, indicating similar concentrations of the galaxy irrespective of the filter. Typical values of C range from 2–5, where $C > 4$ is mainly found for elliptical, while disk galaxies have concentrations between 3 and 4.

(2) *Asymmetry:* Galactic asymmetries can be obtained by rotating the image, centered on the galaxy, by 180° and subtracting this rotated image from the original one. In practice, this is quantified by

$$A = \min\left(\frac{\Sigma\,|I_{\rm rot} - I_0|}{\Sigma\,|I_0|}\right) - \min\left(\frac{\Sigma\,|B_{\rm rot} - B_0|}{\Sigma\,|I_0|}\right). \qquad (2)$$

Here, $I_{\rm rot}$ and I_0 refer to the rotated and original images, respectively, and the summation over the fluxes is carried out within $1.5 \times r(\eta = 0.2)$ as above. *B* denotes the analogous contributions from a background field at sufficiently large
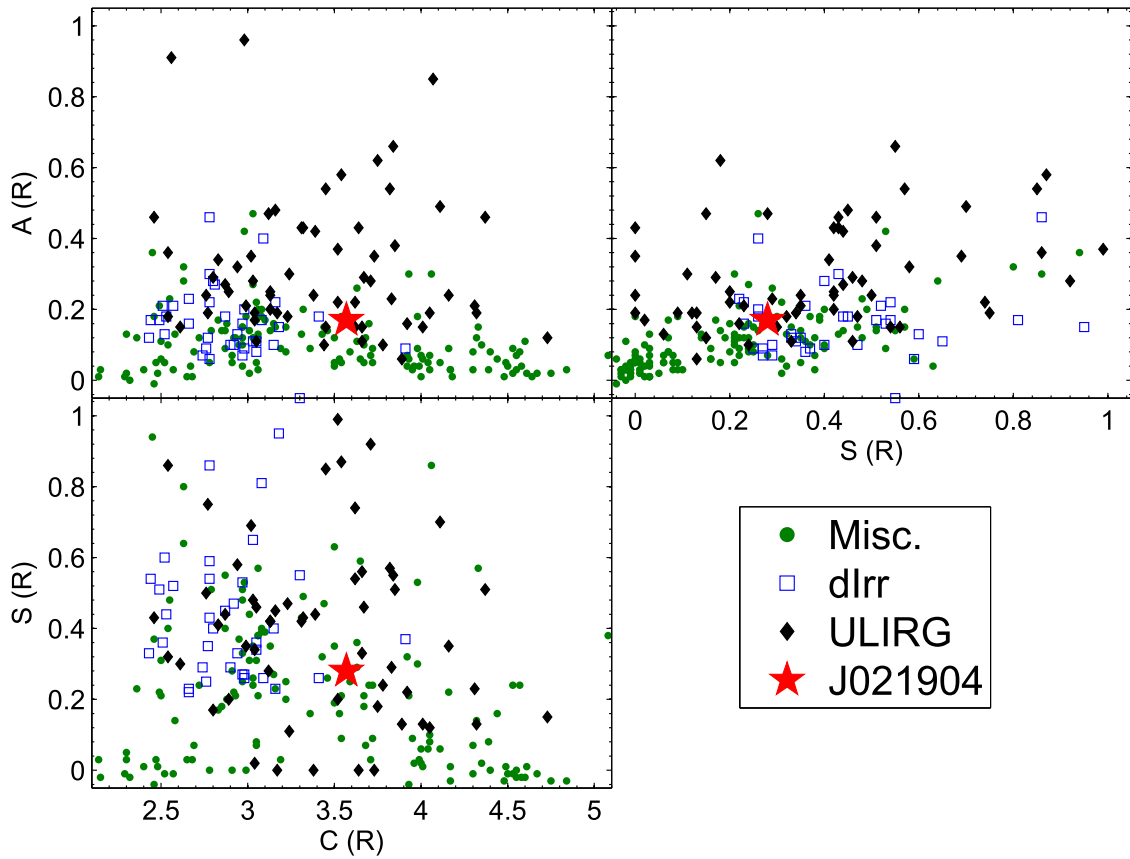
Figure 5. Concentration, asymmetry, and clumpiness parameters of various galaxy types from Conselice ([2003](#)). Our measurement for J021904 from the *V*-image is indicated as a red star symbol. Under "Misc." we grouped Conselice's ([2003](#)) samples containing giant ellipticals/S0s, early- and late-type spirals, and starburst and dwarf elliptical galaxies.

distances that is free from real galactic structures and is introduced to account for contributions from uncorrelated noise. Finally, the minimization was employed so as to optimize the galaxy centroid (Conselice et al. [2000](#)). The asymmetry of J021904 was thus found to be A = (0.15, 0.17, 0.13) in *B*, *V*, and *I*. Given the above definition of A, values around zero would indicate symmetry, whereas an A of unity is caused by large, asymmetric structures. It is noteworthy that there is no significant difference in A between the three different filters we investigated, which could be expected if localized star formation in the galaxy would incur varying asymmetry in different bands.

(3) Clumpiness: High-frequency variations in a galaxy, i.e., any form of clumpy substructures, can be investigated by subtracting a smoothed version of the image from the original one. Following Conselice ([2003](#)), we smoothed our images, I_0 with a kernel of width $0.3 \times r(\eta = 0.2)$ (resulting in I_σ and accounted for the background noise by introducing the same term B_0 as above (Equation ([2](#))):

$$S = 10 \times \left[\left(\frac{\Sigma I_0 - I_\sigma}{\Sigma I_0} \right) - \left(\frac{\Sigma B_0 - B_\sigma}{\Sigma I_0} \right) \right]. \qquad (3)$$

Here, we found S = (0.13, 0.28, 0.16) from the *B*, *V*, and *I* images of J021904.

In Figure [5](#) we put our measurements into context by using the galaxy samples of Conselice ([2003](#)), who established a new classification scheme of galaxies based on these CAS parameters. While the literature values are based on R-band images, we nonetheless overplot our results from the *V*-images, considering that the variations of CAS between our three filters were found to be negligible. Despite its visually irregular nature, the asymmetry of J021904 is moderate and only a few of the dIrrs from Conselice ([2003](#)) fall into the same parameter space as our galaxy. A strong overlap is found for regular galaxies, such as edge-on disks, which, however, can be refuted by the visual appearance on our images. There are, however, also several ultraluminous infrared galaxies found at similar parameter combinations; these show, on average, the largest asymmetries due to the active evolution of these systems, often correlated with ongoing major merger activities. While not extreme in CAS, J021904's asymmetry and clumpiness are consistent with such a merger notion.

Finally, it is also important that Conselice et al. ([2000](#)) note that objects will appear less asymmetric when poorly resolved. At the large distance and small apparent size of the galaxy in question, it is possible that the asymmetry is underestimated from our images, placing it further into the regime of interacting galaxies.

4. SPECTROSCOPIC MEASUREMENTS

Figure [6](#) shows the flux calibrated spectrum, shifted to the rest frame. Several strong emission lines are clearly seen and we identified 10 lines that were significantly measurable above the noise. The first thing to note is that all lines show an asymmetry or are evenly split into two components as in the
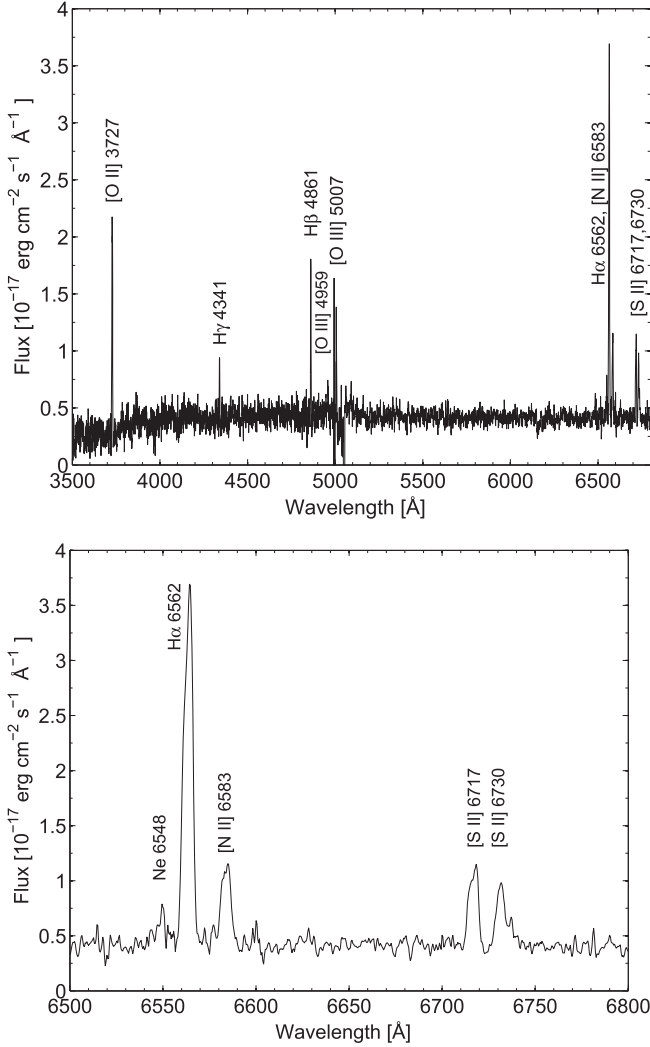
Figure 6. Flux-calibrated MODS spectrum of J021904, converted to the rest frame. The bottom panel shows a zoom around the Hα, [II] λ6584, and the [S II] λλ6717,6730 features. Note the asymmetries in these strong lines.

Table 3
Emission Line Fluxes

Feature	Corrected flux F_0 (10^{-17} erg cm^{-2} s^{-1})
[S II] λ6730	9.27 ± 0.17
[S II] λ6717	9.76 ± 0.17
[N II] λ6584	12.20 ± 0.18
Hα λ6563	46.53 ± 0.15
Ne λ6548	3.64 ± 0.10
[O III] λ5007	11.28 ± 1.02
[O III] λ4959	5.01 ± 0.87
Hβ λ4861	16.27 ± 0.70
[O III] λ4363	<0.51[a]
Hγ λ4340	6.29 ± 0.96
Hδ λ4102	2.7:[b]
[O II] λ3727	58.52 ± 1.51

Notes.
[a] 1σ upper limit.
[b] Uncertain value due to continuum placement.

case of the [O III] 4959 line. Using IRAF's *splot* task we deblended the lines and could measure a systematic split of 142 ± 6 km s^{-1}, which we will further discuss in Section 5. While the resolution of our spectra is sufficient to detect the asymmetries in the line shifts, it is not enough to accurately deconvolve the lines into two separate components and to reliably determine individual line fluxes. Thus we continue with measuring the flux via numerical integration of the emission lines from the spectra after correction for local continuum. The errors on the observed fluxes, in turn, were estimated from the variance spectrum via repeated integration of the lines in a Monte Carlo sense.

4.1. Redshift and Distance

Based on the shifts of 10 prominent emission lines, determined from Gaussian fits using the *splot* task, we obtained a redshift for J021904 of 0.116472 ± 0.000049. This value is in excellent agreement with the photometric redshift from SDSS of 0.132 ± 0.031. Adopting a Hubble constant of $H_0 = 67.8 \pm 0.9$ km s^{-1} Mpc^{-1} and the cosmology derived by the Planck Collaboration et al. (2015) this corresponds to a luminosity distance of 559 ± 7 Mpc (Wright 2006); in turn, $1''$

equals 2.2 kpc at this distance and the pixel size on our WIYN images is 305 pc.

4.2. Extinction, Electron Temperature, and Density

In order to derive the entire color excess due to dust extinction, $\langle E_g(B - V)\rangle$, averaged over the slit, we followed Pasquali et al. (2011) in measuring the Balmer decrement in terms of the observed flux ratio of the Hα and Hβ lines. Since there is only marginal evidence for stellar absorption around the Hγ and Hδ lines, the underlying stellar absorption was deemed negligible. Thus we determine

$$\langle E_g(B - V)\rangle = -\frac{\log(R_{\text{obs}}/R_{\text{int}})}{0.4\left[\kappa(\lambda_{\text{H}\alpha}) - \kappa(\lambda_{\text{H}\beta})\right]}, \qquad (4)$$

where R_{obs} and R_{int} refer to the observed and intrinsic line flux ratios, Hα/Hβ. For the theoretical value we assume $R_{\text{int}} = 2.86$ for case B recombination (Osterbrock & Ferland 2006). Moreover, $\kappa(\lambda)$ was evaluated from the extinction law of Fitzpatrick (1999) at the respective wavelengths of the Balmer lines (see also Calzetti 2001). As a result, we found a total, i.e., intrinsic plus foreground, reddening of 0.43 ± 0.04 mag. Since the Schlafly & Finkbeiner (2011) maps indicate a Galactic foreground reddening of $E_G(B-V) = 0.19$ mag, this leaves an intrinsic $\langle E_g^i(B - V)\rangle$ of 0.24 mag. The overall large extinction (note that $A_V = 1.33$ mag) is likely even underestimating the true value, since such large amounts of dust will attenuate further flux from the inner parts of the galaxy, disabling their use for our extinction estimates.

Finally, the observed emission line fluxes were de-reddened via

$$F_0(\lambda) = F_{\text{obs}}(\lambda) \times 10^{0.4\langle E_g(B-V)\rangle \kappa(\lambda)} \qquad (5)$$

and we list these values in Table 3.

Since the auroral [O III] line at 4363 Å is too weak to be seen in the MODS spectrum, we cannot obtain a direct estimate of the electron temperature, T_e, of the gas phase from the common [O III] $I(\lambda4959+\lambda4959)/I(\lambda4363)$ indicator. Likewise, no other high-excitation, T_e-sensitive emission lines such as [O II] λ7320 or [N II] λ5755 could be significantly detected. We therefore

Table 4
Spectroscopically Derived Characterization of J021904

Parameter	Value
[S II] 6717/6731	1.05 ± 0.03
[O III] (5007+4959)/4363	>33.2[a]
R_{23}	3.94 ± 0.20
O3N2	0.42 ± 0.47
$\langle E_g^i (B - V) \rangle$	0.43 ± 0.04 mag
n_e	430 ± 50 cm^{-3}
T_e	<23000 K[a]/$\lesssim 7000$ K[b]
$12 + \log(\mathrm{O/H})$ (from R_{23})	8.84 ± 0.02 dex
$12 + \log(\mathrm{O/H})$ (from O3N2)	8.59 ± 0.15 dex
L(Hα)	$(1.74 \pm 0.04) \times 10^{40}$ erg s^{-1}
SFR	$(9.2 \pm 1.6) \times 10^{-2}\ M_\odot$ yr^{-1}
M_* (from SFR)	$(5.4 \pm 1.0) \times 10^{8}\ M_\odot$
M_* (from O/H)	$(3.9^{+0.6}_{-0.5}) \times 10^{9}\ M_\odot$
M_* (from fundamental plane)	$(2.1^{+1.2}_{-0.8}) \times 10^{9}\ M_\odot$
M_* (from SED)	$(4.3^{+1.5}_{-1.0}) \times 10^{9}\ M_\odot$

Notes.
[a] 1σ limit based on the upper limit on the [O III] 4363 flux.
[b] Low-excitation estimate based on the non-detection of the [O III] 4363 line.

conclude that the blue, western component of J021904 consists of a low-excitation, metal-rich region, where cooling can proceed via metal lines. Here, electron temperatures are typically found to be on the order of ∼5000–7000 K.

For an estimate of the electron density, n_e, we employed the [S II] $I(\lambda 6717)/I(\lambda 6730)$ ratio and the low T_e adopted above, which yields a typical n_e of 430 ± 50 cm^{-3}. All spectroscopically derived parameters are listed in Table 4.

4.3. Oxygen Abundance

The presence of several strong emission lines in the spectrum of J021904 allowed us to estimate the metallicity of this galaxy from the O3N2 indicator (Alloin et al. 1979), defined as

$$\mathrm{O3N2} = \log \frac{[\mathrm{O\ III}]\,\lambda 5007/\mathrm{H}\beta}{[\mathrm{N\ II}]\,\lambda 6583/\mathrm{H}\alpha}. \tag{6}$$

Pettini & Pagel (2004) devised an empirical calibration of this ratio from a sample of extragalactic HII regions and yielded consistent results with a broad variety of other indicators, discussed, e.g., by Kewley & Dopita (2002). Thus the oxygen abundance of J021904 is determined via

$$12 + \log(\mathrm{O/H}) = 8.73 - 0.32 \times \mathrm{O3N2} \tag{7}$$

as $12+\log(\mathrm{O/H}) = 8.59 \pm 0.15$, or $[\mathrm{O/H}] = -0.07 \pm 0.15$ dex, adopting the solar oxygen abundance of 8.66 from Asplund et al. (2009). Since this is an empirical calibration, our derived metallicity is rather insensitive to the adopted values for electron temperature and density (cf. Kewley & Dopita 2002).

Due to its wide application in the literature, we also employed the R_{23} indicator, which reads

$$R_{23} = \frac{[\mathrm{O\ II}]\,\lambda 3727 + [\mathrm{O\ II}]\,\lambda 4959}{\mathrm{H}\beta}. \tag{8}$$

Following the third-order polynomial calibration of this index to the metallicities of 53,000 galaxies by Tremonti et al. (2004), we obtain a higher oxygen abundance for J021904 of 8.84 ± 0.02 dex, bearing in mind discrepancies between the
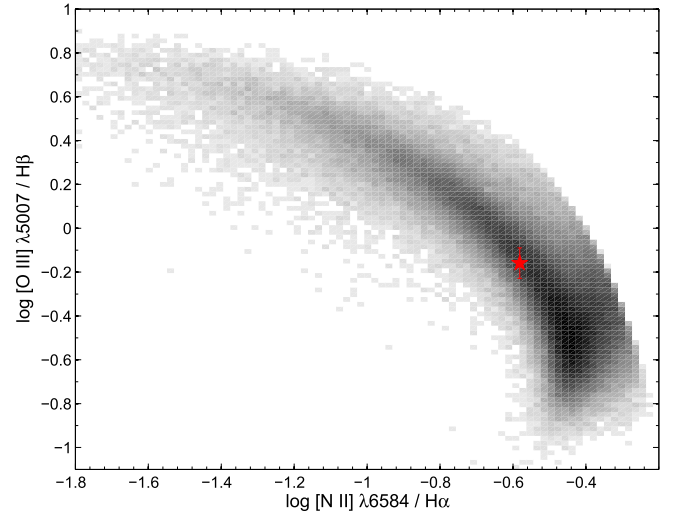

Figure 7. BPT diagnostic diagram, using star-forming galaxies from SDSS (Brinchmann et al. 2004). AGNs have already been pruned from the sample. J021904 is indicated by a red star symbol.

various oxygen abundance indicators (Kewley & Ellison 2008).[10]

4.4. SFR

In Figure 7 we show the diagnostic diagram of (Baldwin et al. 1981; hereafter BPT) for a sample of ∼180,000 star-forming galaxies from SDSS (Brinchmann et al. 2004). Here, using ratios of emission lines close in wavelength efficiently reduces reddening effects. The BPT plot is then a powerful discriminator (e.g., Kewley et al. 2001), taking advantage of the fact that stronger [N II] emission relative to the Hα line is usually indicative of active galactic nuclei (AGNs) while stronger Hα contribution suggests a starburst origin in star formation galaxies. J021904 falls square on the main locus of star-forming galaxies in the BPT diagram, bolstering its earlier identification as a star-forming system.

From our spectrum we derive an Hα-luminosity of L(Hα) = $(1.74 \pm 0.04) \times 10^{40}$ erg s^{-1}. This can be converted into an SFR using the empirical calibration of Calzetti et al. (2007), which reads SFR $[M_\odot$ yr$^{-1}] = 5.3 \times 10^{-42}\,L$(H$\alpha$) [erg s^{-1}] (see also Moustakas et al. 2006 for alternative parameterizations). Thus we find an SFR of $(9 \pm 2) \times 10^{-2}\ M_\odot$ yr^{-1} for the western, blue component of J021904. The quoted uncertainty accounts for the flux-measurement based error on the Hα-luminosity and a 20% variation in the constant of the above relation, as suggested by Calzetti et al. (2007). This low value suggests that J021904 is forming stars at a moderate pace.

4.5. Stellar Mass

There exists a wealth of (stellar-) mass–metallicity, mass–SFR, and metallicity–SFR relations for various types of galaxies (e.g., Lequeux et al. 1979; Tremonti et al. 2004), down to the faintest stellar systems known (e.g., Kirby

---

[10] Template fitting of the Ca II HK absorption lines with pPXF (Cappellari & Emsellem 2004) yielded a consistent, overall metallicity, [M/H], of −0.3 dex. However, we did not pursue the determination of further population characteristics using this method, since all other, e.g., age-sensitive features such as the Mg-b lines are not detectable in the spectrum.
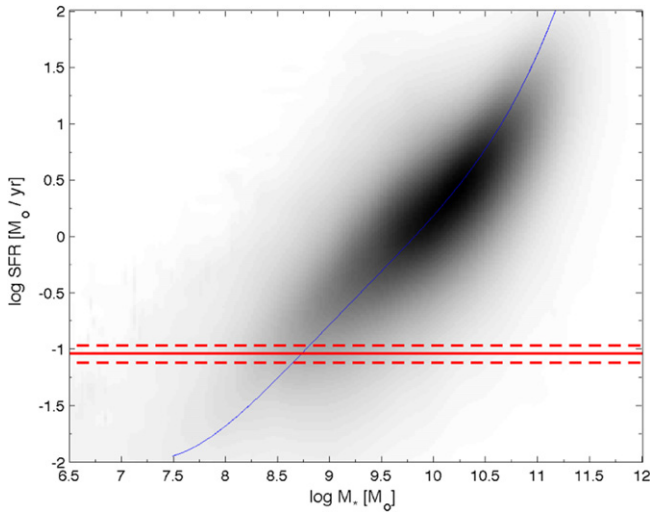
Figure 8. SFR vs. total stellar mass of star-forming galaxies from SDSS (Brinchmann et al. 2004). A polynomial-fit fiducial to those data is shown in blue. Our measurement for J021904 and the 1σ uncertainties are indicated by red lines.

Figure 9. Same as Figure 8, but for the oxygen abundances from Tremonti et al. (2004). The blue line is the second-order polynomial fit to the relation suggested by those authors.

et al. 2011; Koch & Rich 2014). In the following we attempt several measures to estimate the stellar mass of J021904.

(1) *Stellar mass from SFR.* Figure 8 shows the main sequence of star-forming galaxies from SDSS (Brinchmann et al. 2004) in the SFR–stellar mass diagram, where the stellar masses had been derived from the objects' photometry alone (e.g., Kauffmann et al. 2003). Note that this sample is restricted to redshifts between $0.005 < z < 0.22$ so that J021904 representatively lies within this range. Interpolating the fiducial line in this parameter space to the observed SFR for J021904, we obtain a stellar mass of $(5.4 \pm 1.0) \times 10^8 \, M_\odot$.

However, this result should be taken with caution, since masses obtained this way should in principle be corrected for aperture effects that account for differences between the total galaxy luminosity and the flux caught in the fiber (SDSS) or slit (MODS), respectively. For instance, at the median redshift of 0.1 of the SDSS galaxies (Blanton et al. 2003; Brinchmann et al. 2004), the SDSS fibers only sample $\sim 1/3$ of the galaxy light. A possible bias can then be introduced if radial gradients in the galaxy properties are present, predominantly in the *M/L* ratio. While Brinchmann et al. (2004) carefully corrected their large reference sample, we did not further investigate any such aperture effects and will rather resort to more reliable, independent mass indicators in the following.

Finally, we note that, if star formation had been enhanced during the merger event, the actual mass of the unperturbed galaxy would be overestimated with respect to its intrinsically lower SFR value.

(2) *Stellar mass from metallicity.* As above, we interpolated the mass–metallicity relation defined by the SDSS sample of Brinchmann et al. (2004) and Tremonti et al. (2004; their Equation (3)) to the oxygen abundance of J021904. Since Tremonti et al. used the R_{23} indicator as a measure of the oxygen abundance of their sample, for consistency, we used here the abundance of J021904 from the same index (see red lines in Figure 9). This yields a stellar mass for the galaxy of $M_* = (3.9^{+0.6}_{-0.5}) \times 10^9 \, M_\odot$, which is considerably larger than the above estimate from the SFR. However, this estimate is deemed more reliable since the oxygen abundance does not suffer from the biasses due to aperture effects discussed above.
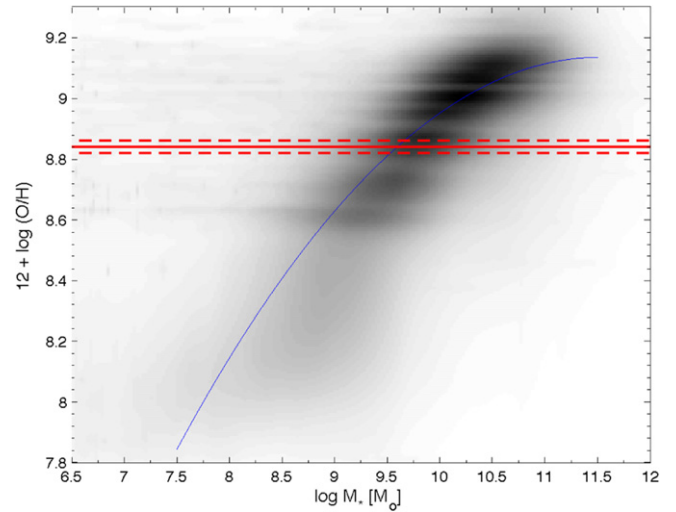
(3) *Fundamental plane.* By combining all of the above parameters of SFR, metallicity (taken as the oxygen abundance), and stellar mass, Lara-López et al. (2010) introduced a fundamental plane for "main-sequence" star-forming galaxies in the field that was based on the SDSS sample we also employed for comparisons above. For J021904, this yields $M_* = (2.1^{+1.2}_{-0.8}) \times 10^9 \, M_\odot$. As for the estimate from the oxygen abundance alone, this result is more reliable compared to the low, SFR-based value, since there are no dependencies on aperture effects. Furthermore, as Lara-López et al. (2010) show, there is no evolution of the fundamental plane with redshift, while there may be such trends within the individual relations (Figures 7, 8; Erb et al. 2006).

(4) *Spectral energy distribution (SED) fitting.* Given the galaxy's faintness (at $g = 19.6$ mag) no photometric information beyond the SDSS magnitudes is available in any other survey such as in the UV (*GALEX*) or the infrared (e.g., 2MASS or *IRAS*). Here we used the MAGPHYS code (da Cunha et al. 2008), which employs the stellar population synthesis models of Bruzual & Charlot (2003) to interpret galaxy SEDs in terms of stellar parameters, also accounting for the properties of the galaxies' dust and interstellar extinction. While emission line spectra are not considered, we obtain a best-fit of the observed SED (Figure 10) of J021904 for a template with a stellar mass of $M_* = (4.3^{+1.5}_{-1.0}) \times 10^9 \, M_\odot$, in line with the estimates from its metallicity and the fundamental relations discussed above. Furthermore, the inferred template metallicity of $Z/Z_\odot$ of 0.62 is in line with our metal-rich value from the O/H measurements.

In conclusion, we find a mean stellar mass of J021904 from all four estimates of $M_* = (3.1^{+1.2}_{-2.5}) \times 10^9 \, M_\odot$, consistent with the typical mass of the LMC and star-forming dwarf galaxies in the Local universe (van der Marel et al. 2002).

5. OVERALL CHARACTERIZATION OF J021904—AN LMC ANALOG?

Depending on the filter used, we found an exponential effective, or half-light, radius of J021904 on the order of 8 kpc, in excellent agreement with the Petrosian radius listed in SDSS. Coupled with its stellar mass and/or absolute magnitude
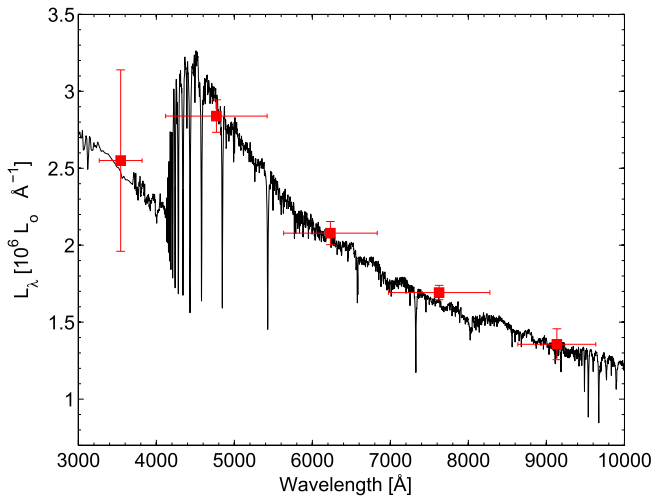
Figure 10. Best-fit SED from the Bruzual & Charlot (2003) models, obtained with MAGPHYS (black). The observed SDSS fluxes are shown in red, where horizontal error bars reflect the filter widths.

estimate, this places this galaxy in the realm of (dwarf) elliptical and Virgo cluster galaxies in the effective radius–mass/magnitude diagrams of, e.g., Misgeld & Hilker (2011; their Figures 1, 4). A deviation of J021904 in these scaling relations toward larger radii can be ascribed to its irregular, merger-induced morphology and the possible tidal features. This compares to a smaller (exponential) radius of 0.7–1.4 kpc of the LMC, which differs with the age of the stellar populations, and its tidal radius of ∼15 kpc (van der Marel 2006, p. 47; Balbinot et al. 2015). In turn, the LMC's H I disk has an extent od 6.5 kpc.

J021904 is characterized by an SFR of $0.09 \, M_\odot \, \mathrm{yr}^{-1}$. This compares with the average, *global* SFR of the LMC of $0.2 \, M_\odot \, \mathrm{yr}^{-1}$, which varied, however, within a factor of two over its history (Harris & Zaritsky 2009). Thus the LMC saw extended, quiescent phases 5–12 Gyr ago, where stars formed at a comparable order of magnitude as seen in J021904. Additionally, it experienced repeated periods of enhanced star formation within the last 3 Gyr, during which the metallicity of the LMC increased by a factor of two (see also Dopita et al. 1997). These peaks were likely triggered by close interactions with the SMC. While the moderate SFR found for J021904 is not unambiguously indicative of a merger-induced star formation activity, the double-cored morphology and emergence of apparent tidal features could suggest that J021904 is currently undergoing a merger within an LMC–SMC-type system.

The metallicity of the LMC has been determined from a large amount of various tracers. The stellar metallicity distribution indicates a metal-poor mean [Fe/H] of −0.6 dex (Cole et al. 2000) with a tail down to approximately −1.8 dex (e.g., Hill et al. 2000). Given the typical [O/Fe] enhancements of the more metal-rich stars in dwarf spheroidal galaxies in the MW-to-solar values and higher enhancements to ∼0.4 dex at the metal-poor end (e.g., Gilmore & Wyse 1991; Shetrone et al. 2001; Koch 2009; Hendricks et al. 2014), the entire covered range would translate to an oxygen abundance on the order of 7.8–8.3 dex. Similarly, oxygen abundances of planetary nebulae have been determined as 8.10 ± 0.25 dex (Stasińska et al. 1998), in line with measurements in H II regions of 8.35 ± 0.06 dex (Russell & Dopita 1992). Moreover, the prominent Magellanic Stream has been characterized as a

metal-poor component, at $12 + \log(\mathrm{O/H}) = 7.46$–7.66 dex (Fox et al. 2013). In comparison, J021904 is a metal-rich system that lies above the nebular abundances for the LMC by at least 0.3 dex, which could indicate that the potential merger happened with an already metal-rich system.

Using three independent, reliable methods, viz., the mass–metallicity relation, the fundamental plane for main-sequence galaxies, and from SED-fitting, we estimated the stellar mass of J021904 to be $3.1 \times 10^9 \, M_\odot$. Considering the large uncertainties on our measurement, this value is in excellent agreement with the total stellar mass of the LMC of $M_{*,\mathrm{LMC}} = 2.9 \times 10^9 \, M_\odot$ (van der Marel et al. 2002).

The line asymmetries seen in the spectrum of J021904 could be due to several dynamic processes, while it is unlikely that we are sampling the depth extent of this object: at the redshift of the galaxy, the split of $140 \, \mathrm{km \, s}^{-1}$ corresponds to ∼2.1 Mpc, which is much larger than the apparent, radial extent of the system on the order of a few tens of kiloparsecs. One viable cause for the splits could be rotation. Both our measured v_{rot} and the inferred mass are in fact consistent with the stellar Tully–Fisher relation observed in local galaxy samples (e.g., Kassin et al. 2007; Miller et al. 2011) and also predicted by simulations of galaxy mergers (Covington et al. 2010). One drawback of this scenario is that due to the orientation of the MODS slit (Figure 3), the observed line split would imply rotation around the major axis or a significant inclination of the system, all of which is feasible if one was to consider the exact geometry of the infalling satellite's orbit. Clearly, future long-slit or IFU observations are needed to settle the relative dynamics of J021904. An alternative could be galactic outflows or spatially separated star-forming regions, as suggested by Pilyugin et al. (2012). Finally, this split could also simply reflect the relative velocities of the merging components on an order of magnitude similar to the (past) relative velocities of the Magellanic clouds.

6. DISCUSSIONS AND CONCLUSIONS

Our discovery of J021904 as an irregular, moderately star-forming, Magellanic galaxy with a complex visual structure brings forth another contender for a major merger event that already acts in the regime of dwarf galaxy masses (see also Rich et al. 2012). In terms of their star-forming properties, Overzier et al. (2008) note that mergers of gas-rich, low-mass ($\sim 10^{10} \, M_\odot$) systems are important triggers of intense star formation activity.

Besla et al. (2012) suggested that many of the LMC structures, such as its warped stellar bar, are a natural outcome of a head-on collision with the lower-mass SMC. These features are an important trademark of the Magellanic Irregulars, indicating that their morphological evolution has indeed been significantly shaped by similar major mergers on the dwarf galaxy scale.

Based on a large sample of galaxy pairs, Davies et al. (2015) found that star formation is enhanced in major mergers and in the primaries of minor mergers, while it is suppressed in the satellites of minor mergers. In fact, our observed line-splitting and its morphology indicate that J021904 contains two star-forming components, revealing a major merger with the bluer, western component we analyzed in this work being the primary, accreting partner. When inferring masses from SFRs, one should then bear in mind that enhanced star formation does not only strictly refer to "star-forming" per se, but that the

galaxy is forming stars more actively than non-merging galaxies of comparable mass.

One open question thus remains if J021904 has evolved as an isolated system or whether it is part of a larger structure such as a galaxy group or cluster. For instance, Tollerud et al. (2011) estimated that 12% of MW-type galaxies host LMC-type satellites within 75 kpc, which corresponds to $34''$ at the distance of our galaxy. For comparison, we thus turn to the Local Group with its (zero-velocity) radius of ~1 Mpc (Karachentsev et al. 2009), which corresponds to $7'.6$ at the distance of J021904. This is essentially comparable to the entire field of view of the MIMO camera (Section 2). Consulting SDSS, we identified eight candidates with photometric redshifts that would place them within a projected radius of 2 Mpc of our Magellanic candidate within their respective errors (note that those are typically on the order of 50%). However, none of them fall within the footprint of our MIMO imaging and the SDSS images of those faint objects indicate no signs of interaction, nor are any of them extended L^* galaxies, so we conclude that J021904 is most likely an isolated, star-forming field galaxy.

REFERENCES

Alam, S., Albareti, F. D., Allende Prieto, C., et al. 2015, ApJS, 219, 12
Alloin, D., Collin-Souffrin, S., Joly, M., & Vigroux, L. 1979, A&A, 78, 200
Asplund, M., Grevesse, N., Sauval, A. J., & Scott, P. 2009, ARA&A, 47, 481
Balbinot, E., Santiago, B. X., Girardi, L., et al. 2015, MNRAS, 449, 1129
Baldwin, J. A., Phillips, M. M., & Terlevich, R. 1981, PASP, 93, 5
Belokurov, V., Walker, M. G., Evans, N. W., et al. 2009, MNRAS, 397, 1748
Bershady, M. A., Jangren, A., & Conselice, C. J. 2000, AJ, 119, 2645
Bertin, E., & Arnouts, S. 1996, A&AS, 117, 393
Besla, G., Kallivayalil, N., Hernquist, L., et al. 2012, MNRAS, 421, 2109
Blanton, M. R., Hogg, D. W., Bahcall, N. A., et al. 2003, ApJ, 594, 186
Boylan-Kolchin, M., Besla, G., & Hernquist, L. 2011, MNRAS, 414, 1560
Brinchmann, J., Charlot, S., White, S. D. M., et al. 2004, MNRAS, 351, 1151
Bruzual, G., & Charlot, S. 2003, MNRAS, 344, 1000
Calzetti, D. 2001, PASP, 113, 1449
Calzetti, D., Kennicutt, R. C., Engelbracht, C. W., et al. 2007, ApJ, 666, 870
Cappellari, M., & Emsellem, E. 2004, PASP, 116, 138
Clark, C. J. R., Dunne, L., Gomez, H. L., et al. 2015, MNRAS, 452, 397
Cole, A. A., Smecker-Hane, T. A., & Gallagher, J. S., III 2000, AJ, 120, 1808
Conn, B. C., Pasquali, A., Pompei, E., et al. 2011, ApJ, 741, 80
Conselice, C. J. 2003, ApJS, 147, 1
Conselice, C. J., Bershady, M. A., & Jangren, A. 2000, ApJ, 529, 886
Covington, M. D., Kassin, S. A., Dutton, A. A., et al. 2010, ApJ, 710, 279
da Cunha, E., Charlot, S., & Elbaz, D. 2008, MNRAS, 388, 1595
Davies, L. J. M., Robotham, A. S. G., Driver, S. P., et al. 2015, MNRAS, 452, 616

Djorgovski, S., & Spinrad, H. 1981, ApJ, 251, 417
Dopita, M. A., Vassiliadis, E., Wood, P. R., et al. 1997, ApJ, 474, 188
Driver, S. P., Norberg, P., Baldry, I. K., et al. 2009, A&G, 50, 12
Eales, S., Dunne, L., Clements, D., et al. 2010, PASP, 122, 499
Erb, D. K., Shapley, A. E., Pettini, M., et al. 2006, ApJ, 644, 813
Fitzpatrick, E. L. 1999, PASP, 111, 63
Forbes, D. A., Beasley, M. A., Bekki, K., Brodie, J. P., & Strader, J. 2003, Sci, 301, 1217
Fox, A. J., Richter, P., Wakker, B. P., et al. 2013, ApJ, 772, 110
Gilmore, G., & Wyse, R. F. G. 1991, ApJL, 367, L55
Harris, J., & Zaritsky, D. 2009, AJ, 138, 1243
Hendricks, B., Koch, A., Lanfranchi, G. A., et al. 2014, ApJ, 785, 102
Hill, V., François, P., Spite, M., Primas, F., & Spite, F. 2000, A&A, 364, L19
Ibata, R., Irwin, M., Lewis, G., Ferguson, A. M. N., & Tanvir, N. 2001, Natur, 412, 49
Ibata, R. A., Gilmore, G., & Irwin, M. J. 1994, Natur, 370, 194
Jordi, K., Grebel, E. K., & Ammon, K. 2006, A&A, 460, 339
Kallivayalil, N., van der Marel, R. P., Besla, G., Anderson, J., & Alcock, C. 2013, ApJ, 764, 161
Karachentsev, I. D., Kashibadze, O. G., Makarov, D. I., & Tully, R. B. 2009, MNRAS, 393, 1265
Kassin, S. A., Weiner, B. J., Faber, S. M., et al. 2007, ApJL, 660, L35
Kauffmann, G., Heckman, T. M., White, S. D. M., et al. 2003, MNRAS, 341, 33
Kelson, D. D. 2003, PASP, 115, 688
Kent, S. M. 1985, ApJS, 59, 115
Kewley, L. J., & Dopita, M. A. 2002, ApJS, 142, 35
Kewley, L. J., Dopita, M. A., Sutherland, R. S., Heisler, C. A., & Trevena, J. 2001, ApJ, 556, 121
Kewley, L. J., & Ellison, S. L. 2008, ApJ, 681, 1183
Kirby, E. N., Lanfranchi, G. A., Simon, J. D., Cohen, J. G., & Guhathakurta, P. 2011, ApJ, 727, 78
Koch, A. 2009, AN, 330, 675
Koch, A., Burkert, A., Rich, R. M., et al. 2012, ApJL, 755, L13
Koch, A., & Rich, R. M. 2014, ApJ, 794, 89
Lara-López, M. A., Cepa, J., Bongiovanni, A., et al. 2010, A&A, 521, L53
Lequeux, J., Peimbert, M., Rayo, J. F., Serrano, A., & Torres-Peimbert, S. 1979, A&A, 80, 155
Liu, L., Gerke, B. F., Wechsler, R. H., Behroozi, P. S., & Busha, M. T. 2011, ApJ, 733, 62
Martínez-Delgado, D., Gabany, R. J., Crawford, K., et al. 2010, AJ, 140, 962
McConnachie, A. W., Irwin, M. J., Ibata, R. A., et al. 2009, Natur, 461, 66
Miller, S. H., Bundy, K., Sullivan, M., Ellis, R. S., & Treu, T. 2011, ApJ, 741, 115
Misgeld, I., & Hilker, M. 2011, MNRAS, 414, 3699
Moustakas, J., Kennicutt, R. C., Jr., & Tremonti, C. A. 2006, ApJ, 642, 775
Osterbrock, D. E., & Ferland, G. J. (ed.) 2006, Astrophysics of Gaseous Nebulae and Active Galactic Nuclei (2nd ed.; Sausalito, CA: Univ. Science Books), 70
Overzier, R. A., Heckman, T. M., Kauffmann, G., et al. 2008, ApJ, 677, 37
Overzier, R. A., Heckman, T. M., Tremonti, C., et al. 2009, ApJ, 706, 203
Pasquali, A., Bik, A., Zibetti, S., et al. 2011, AJ, 141, 132
Pettini, M., & Pagel, B. E. J. 2004, MNRAS, 348, L59
Pilyugin, L. S., Zinchenko, I. A., Cedrés, B., et al. 2012, MNRAS, 419, 490
Planck Collaboration, Ade, P. A. R., Aghanim, N., et al. 2015, arXiv:1502.01589
Pogge, R. W., Atwood, B., Brewer, D. F., et al. 2010, Proc. SPIE, 7735, 77350A
Rich, R. M., Collins, M. L. M., Black, C. M., et al. 2012, Natur, 482, 192
Robotham, A. S. G., Baldry, I. K., Bland-Hawthorn, J., et al. 2012, MNRAS, 424, 1448
Russell, S. C., & Dopita, M. A. 1992, ApJ, 384, 508
Schlafly, E. F., & Finkbeiner, D. P. 2011, ApJ, 737, 103
Shetrone, M. D., Côté, P., & Sargent, W. L. W. 2001, ApJ, 548, 592
Stasińska, G., Richer, M. G., & McCall, M. L. 1998, A&A, 336, 667
Tollerud, E. J., Boylan-Kolchin, M., Barton, E. J., et al. 2011, ApJ, 738, 102
Tremonti, C. A., Heckman, T. M., Kauffmann, G., et al. 2004, ApJ, 613, 898
van der Marel, R. P. 2006, in Proc. STSI Symp., Vol. 17, The Local Group as an Astrophysical Laboratory, ed. M. Livio & T. M. Brown (Cambridge: Cambridge Univ. Press), 47
van der Marel, R. P., Alves, D. R., Hardy, E., & Suntzeff, N. B. 2002, AJ, 124, 2639
van der Wel, A., Straughn, A. N., Rix, H.-W., et al. 2011, ApJ, 742, 111
van Dokkum, P. G. 2001, PASP, 113, 1420
Williams, R. J., Quadri, R. F., & Franx, M. 2011, ApJL, 738, L25
Wright, E. L. 2006, PASP, 118, 1711
Wuyts, S., Förster Schreiber, N. M., van der Wel, A., et al. 2011, ApJ, 742, 96